

Soft-state biomicrofluidic pulse generator for single cell analysis

Poorya Sabounchi, Cristian Ionescu-Zanetti, Roger Chen, Manjiree Karandikar, Jeonggi Seo, and Luke P. Lee^{a)}

Biomolecular Nanotechnology Center, Berkeley Sensor & Actuator Center, Department of Bioengineering, University of California, Berkeley, Berkeley, California 94720-1762

(Received 8 November 2005; accepted 16 March 2006; published online 2 May 2006)

We present the design, fabrication, and characterization of a soft-state biomicrofluidic pulse generator for single cell analysis. Hydrodynamic cell trapping via lateral microfluidic junctions allows the trapping of single cells from a bulk suspension. Microfluidic injection sites adjacent to the cell-trapping channels enable the pulsed delivery of nanoliter volumes of biochemical reagent. We demonstrated the application and removal of reagent at a frequency of 10 Hz with a rise time of less than 33 ms and a reagent consumption rate of 0.2 nL/s. It is shown that this system operates as a low-pass filter with a cutoff frequency of 7 Hz. © 2006 American Institute of Physics.

[DOI: [10.1063/1.2195106](https://doi.org/10.1063/1.2195106)]

Microfluidic devices are becoming popular tools for performing high throughput cell-based assays due to significant advantages in multiplexing, rapid analysis, and reduced reagent consumption.¹ Within cell-based sensing, single cell analysis is inherently more accurate than sensing that relies on ensemble-averaged experiments. Recently, a few studies have demonstrated biofluidic applications specific integrated circuits (BASICs) to perform single cell experiments.²

The ability to precisely deliver small amounts of biochemical reagent is a critical issue in many cell-based assays.³ Kinetic studies of cellular processes are usually carried out using continuous perfusion systems with relatively slow exchange times.⁴ However, parameters that are measured using slow perfusion can be misleading. For instance, an apparent linear response to a biochemical signal could, in fact, result from the desensitization of some receptors which have switched to an inactivated state after opening due to exposure to a ligand.⁵ To effectively study the response, the perturbations must be rapid compared to the relaxation time of the system (i.e., milliseconds to seconds). To achieve this, it is necessary to apply biochemical reagents in a pulsatile manner to the extracellular space.

Traditional pulsed compound application is accomplished by micromanipulated motion of a pair of closely spaced fluid streams across a cell trapped by a pipette under a microscope⁶ or by laser-pulse photolysis.⁷ In a piezobased solution switcher two streams of fluid leave a dual channel glass pipette in laminar flow with two different ligand concentrations (usually a zero and a test concentration). In order to switch solutions, the pipette is rapidly translated normal to its axis, sweeping the flows across a trapped cell at the end of a pipette.⁶ Although this technique is able to collect kinetic ion channel data, it requires a complex and expensive setup and is not widely used for studying dynamics in systems biology.⁸ In order to increase the throughput of this technique, Orwar and co-workers replaced the dual stream scanning probe with several parallel microfluidic channels that create different laminar flowing streams in open volumes to study fast kinetic interactions on the cell surface.⁹ Because it is difficult to maintain a fixed distance between the trapped

cell and the perfusion exit ports, it is difficult to collect accurate data using mechanical scanning. The drawbacks to this technique are the relatively low throughput and complex experimental setup.

We recently introduced a microfluidic platform for electrophysiology in which lateral cell trapping junctions enable hydrodynamic trapping of cells from the bulk cell suspension and electrophysiological recording.¹⁰ In this letter, we present the design and testing of a soft-state biomicrofluidic pulse generator and its integration with a cell trapping array for the simultaneous electrical and optical characterization of the dynamics of cell membrane proteins. A programmable solenoid valve provides the upstream pressure pulses controlling flow in the injection channel, while a constant buffer flow applied in the main channel is used to direct the reagent to the cell and to remove it at the end of each pulse [Fig. 1(a)]. The experimental conditions used here are characterized by low-Reynolds and high-Peclet numbers, which result in efficient solution exchange and inhibit diffusion of biochemical reagent to the buffer flow.

We fabricated our device using soft lithography [Fig. 1(b)]. First, SU-8 2002 (Microchem Corporation) was spin coated and patterned on a silicon wafer to define the 3- μ m height of trapping channels. Then, a 40- μ m SU-8 2050 layer was spin coated and patterned on top of the small channels for main flow channel and injection site. PDMS (Sylgard 184, Dow Corning Corporation) was prepared with a 10:1 ratio between the base and the curing agents. The poly dimethyl siloxane (PDMS) was then poured on the two-level SU-8 mold. The mold was degassed in a vacuum chamber for 10 min before curing in a 70 °C oven for 4 h. The device was then diced by a razor blade and the fluidic connection ports were punched using an 18-gauge flat tip needle. The device was then irreversibly bonded to a coverglass (Fisher Scientific) after oxygen plasma treatment (PlasmaTherm Etcher, 50 W, 2 torr, 40 sec) on both the bottom of the device and the glass slide.

In order to demonstrate biochemical pulse generator around single cells we used a suspended tumor cell line (HeLa). Cells were grown in DMEM+10% FBS (Gibco) and passaged twice weekly. Phosphate buffered saline (PBS) was obtained from Sigma—Aldrich (St. Louis, MO). Nonadherent cells are sequentially brought to the side channels and trapped by applying negative pressure (28 kPa) (Ref. 8).

^{a)}Corresponding author: Department of Bioengineering, University of California, Berkeley, 485 Evans Hall #1762, Berkeley, CA 94720-1762; electronic mail: lpLee@berkeley.edu

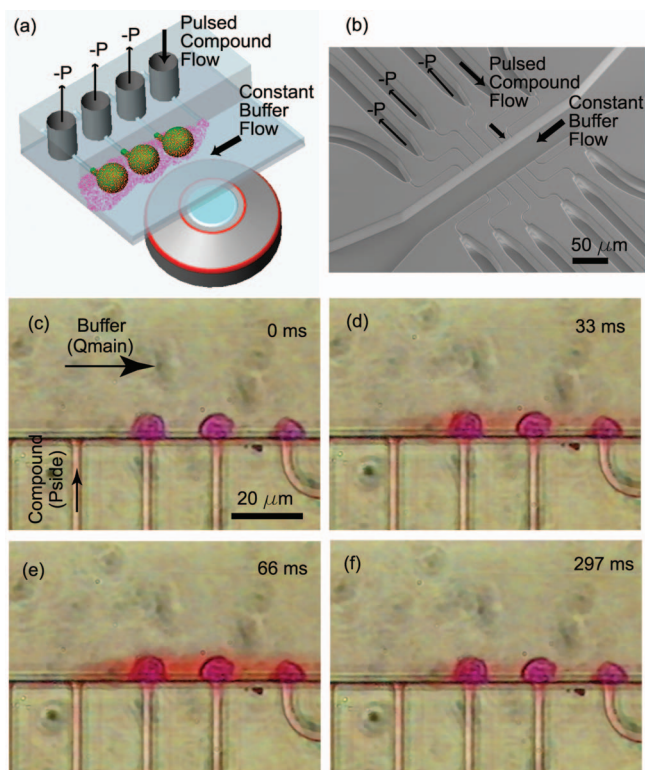


FIG. 1. (Color) (a) Schematic diagram of the soft-state biochemical pulse generator integrated with a cell trapping array. Negative pressure is applied to the side channels to trap the cells. A programmable solenoid valve (not shown) provides the upstream pressure pulses controlling flow in the injection channel. A constant buffer flow applied in the main channel is used to direct the reagent to the cell and to remove it at the end of each pulse. (b) Fabricated device geometry. An SEM image of the microfluidic device before bonding. The main fluidic channel is 50 μm in height. Each side channel had a width of 3 μm and a height of 3 μm . (c–f) Chronological sequence of application and removal of colored dye around trapped single cells for 1 Hz pulsed flow. Reagent application (0%–90% concentration) is achieved in approximately 33 ms (one video frame).

Subsequently, buffer solution is flown through the main fluidic channel at a constant flow rate (2 $\mu\text{L}/\text{min}$) (Cole Parmer 74900). After cell trapping, the solenoid valve pulses biochemical reagents through the injection channel to induce the rapid succession response of single cells [Figs. 1(c)–1(f)].

We developed a finite element model for simulation of steady-state mass transfer characteristics of the device. The finite element model was built using the FEMLABTM software package (version 3.0, Comsol, Stockholm, Sweden). First, the Navier-Stokes equations were solved for the carrier liquid to obtain the flow field. This field was then fixed and the simulation of the convection-diffusion equation was performed. The dimensions of the domains are equal to the values chosen in the preceding section. The entire domain was meshed using four-noded tetrahedron with a dense mesh in the region of larger gradient [Fig. 2(a)]. The solutions were found to be practically independent of the spatial and temporal discretization with the grids used. This was assessed for the three-dimensional (3D) simulations by coarsening and refining the grid spacing by a factor of 2 and repeating the calculation. As the boundary condition, a fully developed velocity profile was imposed at the inlet with maximum velocity corresponding to the inlet flow rate (2 $\mu\text{l}/\text{min}$). Zero traction and no-slip boundary conditions were set at the outlet and on the walls, respectively. In the mass transfer simulation, the carrier liquid in the main channel was modeled as

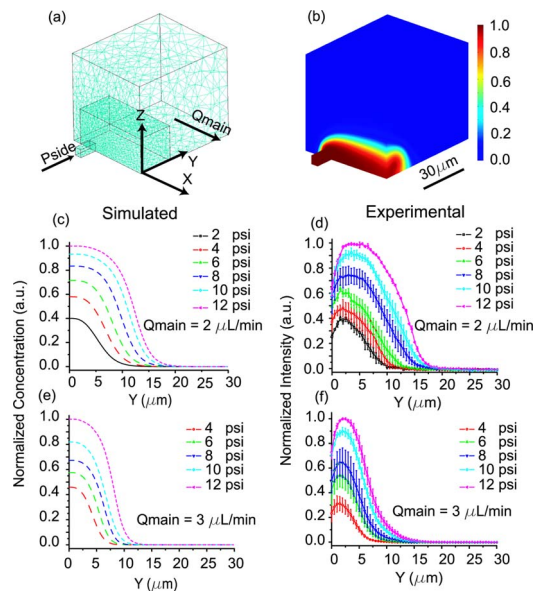


FIG. 2. Steady-state concentration distribution. (a) Discretization of the simulation domain, a denser mesh is used in the regions of larger gradient (plume). (b) 3D plume concentration profile. (c–f) Closeups of the measured intensity profile together with the corresponding simulated profiles for (c and d) 2 $\mu\text{L}/\text{min}$ and (e and f) 3 $\mu\text{L}/\text{min}$ in the main channel at various pressures of the side channel. The simulated concentration results are the integral over vertical section (z). The experimental result is from the intensity profile of 10 nM fluorescein measured 30 μm from the injection channel. The error bars represent the standard deviation for three different devices.

water at 293 K and the compound (fluorescein) at the side channel with a diffusion coefficient $D=1 \times 10^{-10} \text{ m}^2 \text{ s}^{-1}$ to simulate the 3D plume profile [Fig. 2(b)]. Plume intensity distribution of 10 nM fluorescein has been also measured 30 μm from the injection channel for different injection pressures at two different flow rates [Figs. 2(d) and 2(f)]. In order to compare the simulation with experimental results, a cross section of the numerical concentration distribution 30 μm from the injection channel was integrated over the height of the channel [Figs. 2(c) and 2(e)]. The average standard deviation between the normalized intensity measurement and simulated concentration profiles for the two flow rates 2 and 3 $\mu\text{l}/\text{min}$ are 0.0238 and 0.0248, respectively. The greatest discrepancy occurs close to the channel sidewall (at small Y values) and can be explained by the light refraction from the channel wall. These results allow us to calculate the fluidic resistance of the system in a steady-state condition. The *fluidic resistance* is defined as the ratio of hydrodynamic pressure over volume flow rate. Our soft-state microfluidic device exhibits a nonlinear resistance due to expansion of the PDMS channel cross section under pressure.

In order to characterize the biochemical pulses, i.e., reagent exchange efficiency, a fluorescent marker (10 nM fluorescein) was introduced through the injection channel using an upstream solenoid valve (VHS-Nanoliter Dispensing Valves, The Lee Corporation). By monitoring the intensity of fluorescein, we have shown that application and removal can be accomplished at a frequency of 10 Hz, or in a time span of 100 ms. The temporal profile is analyzed by measuring the intensity of a point in the cell trapping region, 30 μm away from the injection channel. Temporal profiles were obtained for various frequencies using an injection pressure of 10 psi, and a main channel flow rate of 2 $\mu\text{L}/\text{min}$ [Fig. 3(a)]. The observed rise time (0%–90%)

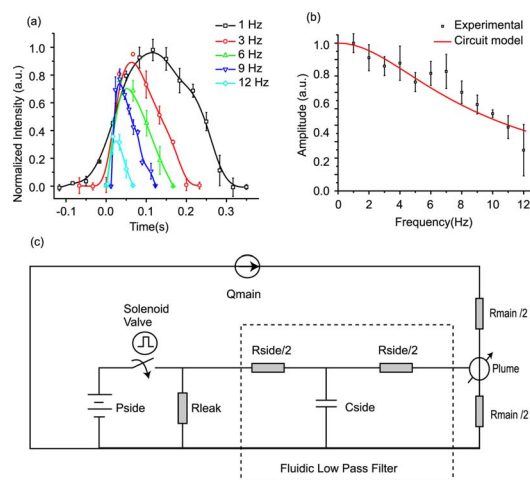


FIG. 3. Pulsed flow characterization. (a) Injection of 10 nM fluorescein measured 30 μm away from the injection channel at various frequencies. The flow rate in the main channel is kept at 2 $\mu\text{L}/\text{min}$ and the pressure upstream of the solenoid valve is kept at 10 psi. The rise time (10%–90%) is less than 33 ms (one video frame) and the reagent consumption rate is 0.2 nL/s. Intensity measurements have been normalized with respect to 1 Hz pulsed flow intensity results. (b) Normalized intensity amplitude of the plume at different frequencies showing a cutoff frequency of 7 Hz. (c) Fluidic circuit model representation of experimental setup. The error bars represent the standard deviation from three different devices.

max concentration) is less than 33 ms, which is the time between consecutive frames for our video acquisition. This result is on par with previously published results using mechanical scanning,⁹ and is one order of magnitude faster than the previously reported microfluidic reagent exchange.³ Reagent consumption per data point is proportional with the flow rate of the reagent in the injection channel and the time of reagent application to the trapped cells. For a measurement time of 500 ms, the reagent volume used is 1.25 nL.

Fast compound exchange is only possible if we use a leak port upstream of the injection channel right after the solenoid valve (i.e., split the exit port of the solenoid valve into two tubes): one tube leading to the injection channel and the other tube leading to ambient pressure. During pulsed application through the injection channel, the PDMS fluidic channels show a capacitive behavior. The combination of capacitive behavior and fluidic resistance of the injection channels causes a pressure-release delay within the device. This creates a fluidic low-pass filter with a cutoff frequency of 7 Hz and prevents the exchange of solutions at higher frequencies [Fig. 3(b)]. In the future, we believe that geometry optimization will make possible application times below 10 ms.

In order to characterize the soft-state microfluidic system, we modeled the device performance using a lumped circuit diagram [Fig. 3(c)]. The fluidic capacitance is described as the ratio of volume change over applied hydrodynamic pressure. Assuming that the channel widens ΔD_H when a hydrodynamic pressure (p) is applied, we can use applications of integral transforms in the theory of elasticity to derive an explicit relationship between pressure and geometry,¹¹

$$P = \frac{4G\Delta D_H}{D_H},$$

where G is the bulk modulus of the microfluidic channels ($G=800$ kPa for PDMS) and D_H is the hydraulic diameter. Therefore we get the fluidic capacitance

$$C = \frac{\Delta V}{P} = \frac{\pi L D_H^2}{8G}.$$

This lumped circuit model is based on the largest resistance and capacitance (RC) elements in the device, which consist of the smallest side channels. These side channels have cross sections of 3 $\mu\text{m} \times 4 \mu\text{m}$ and lengths of 120 μm , and therefore $C=5.7 \times 10^{-21}$ m³/Pa. Using R values calculated from steady-state analysis ($R=1.2 \times 10^{20}$ Pa s/m³) we plotted the normalized concentration amplitude correlated to the circuit response [Fig. 3(b)].

In conclusion, we integrated a soft-state biomicrofluidic pulse generator and a hydrodynamic cell trapping array for the single cell analysis. We demonstrated the application and removal of a reagent to single trapped cells at a frequency of 10 Hz or (a period of 100 ms) with a rise time (0%–90% of max concentration) of less than 33 ms and a reagent consumption rate of below 0.2 nL/s. The local concentration distribution and system fluidic resistance were modeled using finite element calculations based on fluid flow and mass transport equations. It is shown that this system operates as a low-pass filter with a cutoff frequency of 7 Hz, and can be fit by a simple circuit model.

In conjunction with fast solution exchange, such devices will enable the simultaneous monitoring of the binding of fluorescence molecules and the electrophysiological response of cell membrane proteins such as ion channels. The current through ion channels under a pulsed reagent flow can provide vital information on how biochemical signals such as neurotransmitters propagate in synaptic junctions.¹² Further development of the soft-state BASICs presented in this letter will provide a general method for the study of how fast biochemical signals applied to the extracellular space induce changes in biological systems at the single cell level for systems biology investigations.

The devices presented in this paper were fabricated in the U.C. Berkeley Microfabrication Laboratory. Special thanks to Amiral H. Talasaz of Stanford University for help in circuit modeling.

¹D. Beebe and A. Folch, *Lab Chip* **5**, 10 (2005).

²P. J. Lee, P. J. Hung, R. Shaw, L. Jan, and L. P. Lee, *Appl. Phys. Lett.* **86**, 223902 (2005).

³R. Wheeler, W. R. Thronset, R. J. Whelan, A. M. Leach, R. N. Zare, Y. H. Liao, K. Farrell, I. D. Manger, and A. Daridon, *Anal. Chem.* **75**, 3581 (2003).

⁴P. J. Hung, P. J. Lee, P. Sabounchi, R. Lin, and L. P. Lee, *Biotechnol. Bioeng.* **89**, 1 (2005).

⁵B. Alberts, A. Johnson, J. Lewis, M. Raff, K. Roberts, and P. Walter, in *Molecular Biology of the Cell*, 4th ed. (Taylor & Francis, New York, 2002), pp. 831–852.

⁶F. Sachs, *Biophys. J.* **77**, 682 (1999).

⁷L. Niu, R. W. Vazquez, G. Nagel, T. Friedrich, E. Bamberg, R. E. Oswald, and G. P. Hess, *Proc. Natl. Acad. Sci. U.S.A.* **93**, 12964 (1996).

⁸H. Kitano, *Science* **295**, 1662 (2002).

⁹J. Olofsson, H. Bridle, J. Sinclair, D. Granfeldt, E. Sahlin, and O. Orwar, *Proc. Natl. Acad. Sci. U.S.A.* **102**, 8097 (2005).

¹⁰C. Ionescu-Zanetti, R. M. Shaw, J. Seo, Y. Jan, L. Y. Jan, and L. P. Lee, *Proc. Natl. Acad. Sci. U.S.A.* **102**, 9112 (2005).

¹¹I. N. Sneddon, in *Applications of Integral Transforms in the Theory of Elasticity*, edited by I. N. Sneddon (Springer, New York, 1975), Chap. A, Sec. 11.

¹²M. V. Jones and G. L. Westbrook, *Trends Neurosci.* **19**, 96 (1996).